Using noble gases to trace groundwater evolution and assess helium accumulation in Weihe Basin, central China

Wen Zhang [a, b, c, d], Yuhong Li [b,*], Fenghua Zhao [a], Wei Han [b], Yan Li [c], Yunpeng Wang [e],

Greg Holland [d], Zheng Zhou [c]

a. College of Geoscience and Surveying Engineering, China University of Mining and Technology, 100083, Beijing, China

b. Xi'an Center, China Geological Survey, 710054, China

c. Lancaster Environment Centre, Lancaster University, LA1 4YQ, UK

d. School of Earth and Environmental Sciences, The University of Manchester, M13 9PL, UK

e. State Key Laboratory of Organic Geochemistry, Guangzhou Institute of Geochemistry, Chinese Academy of Sciences, Guangzhou, 510640, China

Abstract: The severe shortage of helium resources is an impending global problem. However, the helium accumulation processes and conditions favorable for helium enrichment in reservoirs remain poorly understood, which makes helium exploration challenging. Noble gases are good tracers of subsurface fluids provenance, migration and storage, as well as indicators of the nature and quantity of associated phases. In this study the variation of major gases and noble gases data in Weihe Basin provide us with an excellent opportunity to understand the groundwater evolution and helium accumulation processes. Twelve gas samples collected from wellheads of geothermal wells can be classified into three groups, in which Group A has high concentrations of N_2 (58.57% - 91.66%) and He (0.32% - 2.94%); Group B has high contents of CH_4 (52.94% and 69.50%) and low concentrations of He (0.057% and 0.062%); Group C has a high content of CH_4 (71.70%) and He (2.11%). Helium isotopic ratios are predominantly radiogenic in origin and therefore crustally derived. Measured elemental ratios of noble gases are compared with multiple fractionation models for Group A and B samples, implying that open system heavy oil-water fractionation with excess heavy noble gases has occurred in the basin with V_{oil}/V_{water} ratios of 0.06-0.18. The amount of helium in Group A and B samples requires the release of all ^{4}He produced in the crust since

---

* Corresponding author
E-mail address: L1763@tom.com (Yuhong Li); wenzhangcn@outlook.com (Wen Zhang) Tel: +8618734130189 (Yuhong Li)

28   0.30Ma-1.98Ma into the groundwater. The Group C sample requires an additional He flux from

29   adjacent granitic bodies. The accumulation of helium and hydrocarbon in the Weihe Basin can be

30   explained by a 4-stage process. Accumulation of commercially viable helium requires high He flux

31   from source rocks, the existence of a free gas phase of major gas components (CH_4 in most cases,

32   N_2 or CO_2) and minimal major gas addition after formation of the free gas phase.

33   **Keywords:** Noble gases; Helium accumulation; Oil-water fractionation; Weihe Basin

34

35   **1. INTRODUCTION**

36   Helium is an essential resource used extensively in nuclear magnetic resonance (NMR),

37   high-tech industries and scientific research (Cai et al., 2010). Based on present global helium

38   reserves, a severe shortage of helium is imminent (Nuttall et al., 2012; USGS, 2018), making

39   helium resource exploration an urgent issue.

40   ^{4}He production is dominated by α-decay of ^{235,238}U and ^{232}Th in sedimentary strata, basement

41   or crust (Ballentine and Burnard, 2002; Brown, 2010). The ^{4}He release process is controlled by two

42   mechanisms: (1)^{4}He is released from crust or aquifer by steady-state flux and accumulated in

43   groundwater (Torgersen and Clarke, 1985; Torgersen and Ivey, 1985; Castro et al., 1998), making

44   ^{4}He an effective tool to date groundwater associated with oil and gas reservoirs (Barry et al., 2017;

45   Zhou and Ballentine, 2006) and ancient fluid systems (Holland et al., 2013). (2)^{4}He can also be

46   liberated rapidly over a short period of time from ancient rocks by magmatic and tectonic activity,

47   as shown at Yellowstone in the U.S.A. (Lowenstern et al., 2014) and Tanzania (Danabalan, 2017).

48   After release, the concentration of ^{4}He in the subsurface fluid systems can then be altered by

49   interactions with oil, gas and water. Helium is often associated with natural gas (Ballentine and

50   Lollar, 2002; Brown, 2010), nitrogen (Danabalan et al., 2016), and carbon dioxide (Gilfillan et al.,

51   2008) and can be closed linked to groundwater flow, as observed in the Hugoton-Panhandle gas

52   field (Ballentine and Lollar, 2002; Danabalan, 2017).

53   Noble gases have been widely used in hydrocarbon systems to quantify oil-water-gas

54   interaction during groundwater movement and hydrocarbon accumulation (Ballentine et al., 1991;

Barry et al., 2016; Wen et al., 2015; Zhou et al., 2005) as well as in CO_2 and N_2 systems (Ballentine and Lollar, 2002; Danabalan, 2017; Gilfillan et al., 2008; Zhou et al., 2012) because of their chemical inertness. In these case studies, noble gases dissolved in air-saturated water (ASW, water that has equilibrated with air under recharge conditions) are transported into the subsurface preserving ASW noble gas signatures, which are subsequently modified by solubility-controlled equilibration when groundwater contacts oil and/or gas phases (Ballentine et al., 2002; Kipfer et al., 2002). Thus ASW-derived noble gases dissolved in groundwater or partitioning into gas phases provide a tool to understand the relationship between groundwater evolution and hydrocarbon and helium accumulation.

In this study, we present the concentrations and isotope ratios of noble gases, major gas components and carbon isotopes of CH_4 and CO_2 in gas samples collected from geothermal wells in Weihe Basin, central China. The combination of these data provides an excellent opportunity to understand the influence of groundwater (traced by ASW-derived noble gases) and major gas components on helium transportation and accumulation as well as determining the sources of helium.

2. GEOLOGICAL SETTING

Weihe Basin, a Cenozoic graben measuring 22000 km^2, is located in central China (Figure 1). It is the southern part of the Cenozoic graben system surrounding the Ordos Block, formed during the continental extension of the Qinling Orogenic Belt (Deng and You, 1985; Li and Ren, 1986). Geophysical data suggest the crustal thickness is around 35-38km under the Weihe Basin compared with 40km beneath the Ordos Basin. There is an upper mantle uplift of 5-6 km under the Weihe Basin (Xu et al., 1993). Neoproterozoic, Paleozoic and Mesozoic granitoid formations occurred throughout the Qinling Orogenic Belt (Wang et al., 2015b), which are rich in uranium and thorium (Han et al., 2014). Many Cenozoic faults and fractures are present in the basin and around the border area, suggesting extension in this region during the Cenozoic (Mercier et al., 2013). Numerous destructive earthquakes, such as the 1556 M8 Huaxian earthquake (Zhang et al., 1995),

82   demonstrate that this region has been tectonically active until very recently.

83   Two main depressions, the Xi'an Depression and the Gushi Depression, are distributed

84   throughout the basin. The basin is filled with Cenozoic strata around 7000m thick, which is

85   comprised of Eocene, Miocene, Pliocene, Pleistocene, and Holocene layers. The major geothermal

86   reservoir is found within the Pliocene Lantian-Bahe Formation, deposited under fluvial to shallow

87   lacustrine conditions (Ma et al., 2010). Groundwater is recharged from the Ordos Basin in the north

88   and the Qinling Orogenic Belt in the south and discharged from the Weihe River in the middle.

89   Sampling wells are distributed in the area of groundwater circulation from the Qinling Orogenic

90   Belt to the Weihe River. Depths of sample collection are listed in Table 1.

91

92   **3. SAMPLING AND ANALYTICAL METHODS**

93   **3.1 Sampling**

94   Twelve gas samples were collected from the wellheads of different producing geothermal wells

95   in the Weihe Basin, 7 of which are located in the Xi'an Depression and 5 are located in the Gushi

96   Depression. A flash tank was equipped at the wellhead of WR-HX to separate gas and water due to

97   the high gas content. Therefore, the gas sample was collected directly from the exhaust pipe for

98   WR-HX. Since there were only gas bubbles exsolved from groundwater at other wellheads and

99   flash tanks are not equipped, a gas-water separator was used to take gas samples (Pinti et al., 2017).

100   Noble gas samples were collected in standard refrigeration grade 10mm external-diameter copper

101   tubes (~50cm in length). The gas was allowed to flow freely through the collection system for at

102   least 10 minutes to remove air contamination before the tubes were sealed by stainless steel

103   pinch-off clamps (Weiss, 1968; Zhou et al., 2005). Additional samples for analysis of major gas and

104   carbon isotopes of CH_4 and CO_2 were collected in upside-down glass bottles by displacing saturated

105   salt water.

106   Gases in Group A and Group B wells are dissolved in groundwater in the subsurface in the

107   Weihe Basin (Zhang et al., 2014a). Because a gas-water separator was used to separate gas and

108   water phases during sampling and the gaseous phase has a strong affinity for noble gases (Warr et

4

al., 2018), a complete degassing of noble gases can be assumed. Therefore, the elemental and isotopic ratios measured in the gas phase of Group A and Group B samples can represent the associated groundwater from which the gases are exsolved. The much higher gas content at the wellhead of Group C well (WR-HX) in comparison to other sampling wells, as well as their associated noble gas signatures suggest that there is a gas reservoir in the subsurface (discussed in section 5.2.2). The sampled gas at the wellhead of WR-HX is a mixture of free gas and dissolved gas.

3.2 Analytical methods

3.2.1 Major gas components and carbon isotopes

Major gas components were analyzed at the Key Laboratory of Petroleum Resource Research, Chinese Academy of Sciences, Lanzhou. The analytical procedures were described in detail in Zhang et al. (2018a). Briefly, the contents of CH_4 and non-hydrocarbon gases were measured by a MAT271 mass spectrometer. CH_4 and other hydrocarbon gases were analyzed on an on-line continuous flow gas chromatograph (Agilent 6890 GC), which is equipped with flame ionization and thermal conductivity detectors. Since CH_4 concentrations were analyzed by both MAT271 and GC, the non-hydrocarbon and hydrocarbon results were calibrated to 100% in total based on the CH_4 contents. The analytical errors were less than 1 vol.% for CH_4, CO_2 and N_2 and less than 10 vol.% for other gases.

Carbon isotopes of CH_4 and CO_2 were measured at the State Key Laboratory of Organic Geochemistry, Guangzhou Institute of Geochemistry, Chinese Academy of Sciences, Guangzhou. The analyses were performed by a Delta Plus II XL GC-IRMS equipped with a CP-Poraplot Q column using standard techniques as described in Gai et al (2019). Each gas sample was analyzed twice and the errors were less than ±0.5‰.

3.2.2 Noble gases

Noble gas analysis was conducted in the noble gas laboratory at Lancaster University. The analytical system can be divided into four sections: sample introduction, sample purification, noble gas separation and noble gas analysis system, which is shown in Figure 2.

After connecting a sample copper tube to the gas extraction line, the line was evacuated through a turbomolecular pump for at least 6 hours to remove air and ensure the prepline vacuum was less than 2×10^{-7} mbar, which was monitored by a compact cold cathode pressure gauge. A quadrupole mass spectrometer (Hiden Analytical HAL-201) was used to further monitor vacuum and check for any leaks from the crimped copper tube. After releasing gas from the copper tube, samples were expanded into a calibrated volume where pressure was recorded by an MKS dual capacitance manometer. Then the sample was transferred to the purification line where hydrocarbons and other reactive gases were removed by titanium sponge initially held at 800 °C for 1min and then cooled to room temperature of 21 °C in 20mins. Further purification was carried on a hot getter (SAES GP-50) held at 250 °C for 15mins. Heavy noble gases (Ar, Kr and Xe) were trapped in a cold finger by charcoal at 77K (refrigerated by liquid nitrogen) and light noble gases (He and Ne) were trapped by a Janis cryogenic trap at 9.5K.

After trapping all noble gases, temperature of the cryogenic trap was increased to 50K and held for 5mins to release helium, which was then admitted to the Isotopx NGX mass spectrometer to measure the helium concentration and isotopic ratio. Neon was subsequently released from the cryogenic trap at 110K and held for 5mins before admittance to the mass spectrometer. Doubly-charged $^{40}Ar^{++}$ and CO_2^{++} were used to correct ^{20}Ne and ^{22}Ne following the methods of Niedermann et al. (1993). After measurements of He and Ne, the charcoal cold finger was heated from 77K to 450K and held for 10mins to release argon, krypton and xenon completely. Two aliquots of the released gas were admitted into NGX mass spectrometer successively for separate analysis of argon and krypton. The remaining Xe in the gas phase was then re-absorbed onto a charcoal trap held at 210K for 10mins followed by pumping out of the residual unabsorbed gas (argon and krypton). Finally, the charcoal trap was heated to 450K and held for 10mins again to release xenon, which was admitted into NGX mass spectrometer for xenon analysis. A cold getter (SAES GP-50) was held at room temperature (21°C) to further remove hydrogen before allowing gases into the mass spectrometer.

A blank and an air standard were analyzed for each sample. Blank corrections for ^{4}He, ^{20}Ne, ^{40}Ar, ^{84}Kr and ^{130}Xe blanks were 0.37 vol%, 0.04 vol%, 0.67 vol%, 0.16 vol% and 0.11 vol% of the average sample size, respectively.

4. RESULTS

4.1 Major gas components and carbon isotopes

Sample names, locations, depths, major gas components and carbon isotopes are listed in Table 1. Seven samples and five samples were collected from the Xi'an and Gushi Depressions respectively. These samples can be classified into three groups based on their CH_4, N_2 and He concentrations. Group A includes all samples collected from the Xi'an Depression (XP-1, XP-2, XP-3, XY-1, XY-2, XY-3 and WG-1) and two samples taken from the Gushi Depression (WR-2 and WR-051). They have relatively low concentrations of CH_4 between 2.23% and 25.40% (9.78% average), high concentrations of N_2 between 58.57% and 91.66% (76.14% average) and high concentrations of He between 0.32% and 2.94% (1.62% average). Group B is composed of two samples from the Gushi Depression (WR-1 and WR-11) with high concentrations of CH_4 (52.94% and 69.50%), low concentrations of N_2 (27.81% and 4.85%) and low concentrations of He (0.057% and 0.062%). Finally, we classify one sample (WR-HX) as Group C as it is characterized by a high concentration of He (2.11%) and similar contents of CH_4 (71.70%) and N_2 (27.20%) compared to samples in Group B. The CO_2 concentrations in the majority of samples are lower than 10% (0.03% - 9.36%, 4.02% in average) except for WR1 (22.24%), WR11 (13.56%), and XY-2 (31.69%). There are minor amounts of other hydrocarbon gases (C_{2-6}) in all samples. O_2 is observed in all samples except for the Group C sample. The carbon isotopic composition of CH_4, $\delta^{13}C(C_1)$, shows a large range from -19.04‰ to -44.46‰ (VPDB). $\delta^{13}C(CO_2)$ values vary between -10.50‰ and -5.47‰, reported relative to Vienna Pee Dee Belemnite (VPDB), which form a positive correlation ($R^2 =$ 0.63) with CO_2 concentrations.

4.2 Noble gases

He, Ne, Ar, Kr and Xe abundances and isotopic compositions of the 12 samples are given in

Table 2. Helium concentrations in Group A and C samples are higher than those in Group B samples by one to two orders of magnitude. Other noble gases in Group A samples show higher concentrations compared with those of Group B and Group C samples. The noble gas signatures are described from section 4.2.1 to section 4.2.5.

4.2.1 Helium

^{4}He concentrations are between 32.3 and 294×10^{-4} cm^3 STP/cm^3 in Group A samples, 5.74 and 6.21×10^{-4} cm^3 STP/cm^3 in Group B samples and 211×10^{-4} cm^3 STP/cm^3 in the Group C sample. The ^{4}He concentrations in the Weihe Basin geothermal field are much higher than those in most natural gas fields around the world. For example, ^{4}He concentrations are $0.04\text{-}116 \times 10^{-6}$ cm^3 STP/cm^3 in the San Juan Basin, USA (Zhou et al., 2005) and $5.32\text{-}6.81 \times 10^{-5}$ cm^3 STP/cm^3 in the Sleipner Vest gas field (Barry et al., 2016) respectively. Helium in the Weihe Basin is dominated by radiogenic components with helium isotope values (^{3}He/^{4}He) varying between 0.033Ra $\pm$ 0.001Ra and 0.126Ra $\pm$ 0.002Ra, where Ra is the atmospheric value of ^{3}He/^{4}He of 1.4×10^{-6} (Mamyrin and Tolstikhin, 1984). Measured ^{4}He/^{20}Ne values are between 1439 and 37164, which are much higher than the ratio in ASW (0.288, Kipfer et al., 2002) or air (0.318, Sano et al., 2013). Therefore, atmospheric or ASW-derived gas has little contribution to ^{4}He concentrations. Using a simple two-component mixing model between a sub-continental lithospheric mantle-like endmember (6.1Ra, Gautheron and Moreira, 2002) and an upper crustal endmember (0.008Ra, Ballentine and Burnard, 2002), the mantle contribution to helium is between 0.40% and 1.94%. The remainder of the ^{4}He is derived from the crust (Fig. 3).

4.2.2 Neon

^{20}Ne concentrations are between 15.9 and 39.5×10^{-7} cm^3 STP/cm^3 (30.0×10^{-7} cm^3 STP/cm^3 in average) in Group A samples, 0.69 and 1.11×10^{-7} cm^3 STP/cm^3 in Group B samples, and 5.50×10^{-7} cm^3 STP/cm^3 in the Group C sample. Measured ^{20}Ne/^{22}Ne ratios vary between 8.68 $\pm$ 0.15 and 10.9 $\pm$ 0.40, showing minor deviations from the atmospheric ^{20}Ne/^{22}Ne value of 9.80 (Bottomley et al., 1984, Fig. 4). This may be due to minor mass fractionation as observed previously (Zhou et al., 2005). Measured ^{21}Ne/^{22}Ne ratios vary between 0.0291 $\pm$ 0.0008 and 0.0311 $\pm$ 0.0008 except for

216 sample WR-HX (0.0385 ±0.0015), compared with the atmospheric value of $^{21}Ne/^{22}Ne=0.029$

217 (Bottomley et al., 1984). Ne isotope ratios are indistinguishable between the samples from the two

218 depressions. Helium isotopes suggest a minor contribution from mantle degassing, therefore the

219 "excess" ^{21}Ne can be accounted for by the addition of radiogenic ^{21}Ne to ASW-derived Ne (Fig. 4).

220 The crustal Ne endmember is featured by $^{20}Ne/^{22}Ne=0$ and $^{21}Ne/^{22}Ne = 0.47$ (Kennedy et al., 1990).

221 Based on the simple two-component mixing model between air and crust (Ballentine et al., 2002),

222 the ^{21}Ne derived from crust accounts for between 0.0% and 9.5% of the total ^{21}Ne except for

223 WR-HX well, which is 33.3%.

4.2.3 Argon

225 ^{36}Ar concentrations range between 7.18 and 19.20×10^{-6} cm^3 STP/cm^3, with $^{40}Ar/^{36}Ar$ ratios

226 varying between 339 ± 5 and 613 ± 11 in Group A samples. Comparatively, Group B samples show

227 around 10 times lower ^{36}Ar concentrations (2.51 and 5.78×10^{-7} cm^3 STP/cm^3) and slightly higher

228 $^{40}Ar/^{36}Ar$ ratios (542 ± 9 to 735 ± 13). The Group C sample shows a higher ^{36}Ar concentration

229 $(2.88\times 10^{-6}$ cm^3 STP/cm^3) and a higher $^{40}Ar/^{36}Ar$ ratio (1142 ± 19) than Group B samples. $^{40}Ar/^{36}Ar$

230 ratios show different deviation from the atmospheric $^{40}Ar/^{36}Ar$ ratio of 298.56±0.31 (Lee et al.,

231 2006; Mark et al., 2011). Resolved excess $^{40}Ar^*$ ($^{40}Ar^* = ^{40}Ar - 298.56 \times ^{36}Ar$, Battani et al., 2000)

232 contributes 12.9%-74.1% to the total ^{40}Ar. Since there is no distinct mantle-derived helium, we

233 assume the excess ^{40}Ar is derived from a radiogenic source. Measured $^{38}Ar/^{36}Ar$ ratios are air-like

234 (0.1885±0.0003, Lee et al., 2006; Mark et al., 2011), varying between 0.180±0.006 and

235 0.200±0.005.

4.2.4 Krypton and Xenon

237 ^{84}Kr concentrations are between 16.6 and 64.8×10^{-8} cm^3 STP/cm^3 in Group A samples and

238 between 0.869 and 2.07×10^{-8} cm^3 STP/cm^3 in Group B samples and 9.95×10^{-8} cm^3 STP/cm^3 in the

239 Group C sample. The isotope ratios of krypton are indistinguishable from corresponding air ratios.

240 For example, $^{86}Kr/^{84}Kr$ ratios range from 0.286±0.014 to 0.322 ± 0.022 compared to the

241 atmospheric ratio of $^{86}Kr/^{84}Kr = 0.3035±0.000008$ (Aregbe et al., 1996).

242 ^{130}Xe concentrations vary from 14.5 to 40.2×10^{-10} cm^3 STP/cm^3 in Group A samples, compared

9

with 0.98 - 2.65 $\times$ 10^{-10} cm^3 STP/cm^3 in Group B samples and 8.17 $\times$ 10^{-10} cm^3 STP/cm^3 in the Group C sample. Samples are featured by air-like Xe ratios, e.g., ^{132}Xe/^{130}Xe ratios vary from 6.47±0.27 to 7.22±0.69 compared to the atmospheric value of 6.6098±0.0023 (Valkiers et al., 1998).

4.2.5 Air contamination

The relationship between noble gas isotopic ratios and noble gas concentrations is an effective tool for estimating air contamination (Barry et al., 2016). Fig. 5 shows the relationship between ^{40}Ar/^{36}Ar and 1/^{36}Ar for all samples (Fig. 5a) and samples only in Group A (Fig. 5b) due to large differences in ^{36}Ar contents among the groups. ^{40}Ar/^{36}Ar ratios show a similar relationship with 1/^{20}Ne values for all samples (not shown in figures). Given the adjacent sample locations of XP-1, XP-2 and XP-3 (maximum distance is 2.3 km) and horizontal strata in this area, it is reasonable to assume similar pristine noble gas signatures for gas samples from the three wells. Since the data of XP-2 and XP-3 are highly consistent with the mixing line of XP-1 and air in Fig. 5b, the two samples were deemed to be contaminated by air and regarded as 'Outlier Samples'. In addition, the ^{20}Ne/^{36}Ar ratios of XP-2 and XP-3 (0.405 and 0.374) are also between the atmospheric value (0.542, Sano et al., 2013) and the ratio of XP-1 (0.295). The concentrations of radiogenic components (^{4}He, ^{40}Ar*) in XP-2 and XP-3 are also lower than those of XP-1 (Table 2). Therefore, it is possible that these two samples were contaminated by air. Since the vacuum integrity of the sample preparation system is monitored by a pressure gauge and a quadrupole mass spectrometer, the air addition during sample processing in the lab can be excluded. Air contamination may have been acquired during sample collection. The following discussion excludes these two samples. There is no positive correlation between ^{40}Ar/^{36}Ar ratios and 1/^{36}Ar values for the remainder of the samples, suggesting that they are unaffected by air contamination.

5. DISCUSSION

5.1 Modelling of groundwater evolution

Atmosphere-derived noble gases (e.g., ^{20}Ne, ^{36}Ar, ^{84}Kr and ^{130}Xe) are dissolved into meteoric water under surface conditions. They are transported into the subsurface system by aquifer recharge.

The absence of other significant subsurface sources makes them ideal tracers for gas-oil-water fractionation in sedimentary basins (Pinti and Marty, 1995; Wen et al., 2015). In this study, noble gas data of Group A and B samples are used to identify phase interactions among oil, gas and groundwater. In addition, the volume ratios of the different phases are quantified as the amount of oil and gas present in a reservoir is key information for hydrocarbon exploration. In this study we also test open system versus closed system models, providing a tool to understand the extent of groundwater circulation and its influence on hydrocarbon and helium accumulation processes.

5.1.1 Modelling conditions

Noble gas concentrations and elemental ratios in air saturated water (ASW) were calculated using Henry's law under recharge conditions of 10°C, 0M NaCl and an average altitude of 1000m in the recharge area (North Qinling Belt). As a result, the initial $^{20}Ne/^{36}Ar$ ratio, $^{84}Kr/^{36}Ar$ ratio and $^{130}Xe/^{36}Ar$ ratio in ASW are taken to be 0.143, 4.02×10^{-2} and 4.02×10^{-4} respectively. The geothermal groundwater is extracted from an approximate depth of 2500m, where the temperature and pressure are taken to be 88°C and 25MPa respectively based on a surface temperature of 13°C, an average geothermal gradient of 30°C/km and a hydrostatic pressure gradient of 10MPa/km. The salinity of groundwater is taken to be 0.1 M NaCl equivalent based on the measured value of 2.0-7.8g/L. The geothermal gradient, hydrostatic pressure gradient and groundwater salinity were measured by Shaanxi Geological Environment Monitoring Station. Henry's constants of noble gases used for modelling are calculated from empirical equations, corrected with fugacity coefficients and activity coefficients (Ballentine et al., 2002 and references therein). The calculated Henry's constants are listed in Table 3.

5.1.2 Gas-water fractionation

Solubilities of noble gases in water increase with mass (Ne < Ar < Kr < Xe) (Ballentine et al., 2002), therefore Ne exsolves into the gas phase most readily whereas progressively heavier noble gases remain dissolved into groundwater. If the gas-water fractionation occurred in the groundwater within the Weihe Basin, the $^{20}Ne/^{36}Ar$ ratios in the water phase would be lower than the initial $^{20}Ne/^{36}Ar$ ratio in ASW. However, all measured $^{20}Ne/^{36}Ar$ ratios in Group A and B samples (0.195 -

11

0.382), which represent the noble gas signatures in the water phase, are higher than the ratio of ASW (0.143). This cannot be explained by the simple gas-water fractionation model.

The possibility of multi stage gas-water fractionation (re-solution and effervescence model, Ballentine et al., 2002) was also considered. A gas phase exsolved from the ASW would have an elevated $^{20}Ne/^{36}Ar$ ratio. When the exsolved gases dissolve into a small volume of water, this process will lead to a significant increase of $^{20}Ne/^{36}Ar$ ratio in the groundwater. Iterative exsolving and dissolving will further increase the $^{20}Ne/^{36}Ar$ ratio in the water phase (Ballentine et al., 2002). Multi stage exsolution and dissolution models require variation in the pressure/temperature conditions in the subsurface, presumably due to repeated uplift and subsidence of strata. However, the Weihe Basin has been mainly subject to extension and settlement continuously since the Palaeogene (Mercier et al., 2013). This is inconsistent with the complex conditions needed for the re-solution and effervescence model. Therefore, we consider that the simple and multi stage gas-water fractionation models are not viable explanations for the noble gas data recorded from the Weihe Basin.

5.1.3 Oil-water fractionation

Oil has been found to adhere in the pipes of geothermal wells in the Gushi Depression and around 50kg of oil are produced from WR-11 and WR-2 through oil water separating equipment per day. Therefore, it is reasonable to consider a model in which the groundwater has been equilibrated with an oil phase earlier during its migration. In addition, the involvement of oil can explain the high $^{20}Ne/^{36}Ar$ value in groundwater since Ar relative to Ne has higher solubility in oil than water (Battani et al., 2000; Zhou et al., 2012). If the oil-water equilibrium process occurs in either a closed system, batch fractionation of noble gases occurs. Conversely, open system equilibration will result in a Rayleigh fractionation pattern of noble gases. Both cases are modelled in this study assuming an oil API of 25 and 34 respectively.

Batch fractionation.

When equilibrium has been achieved under closed system conditions, the elemental ratios of noble gases follow the batch fractionation equation (Ballentine et al., 2002):

324
$$\left(\frac{A}{B}\right)_{water} = \left(\frac{A}{B}\right)_{ASW} \times \left(\frac{\frac{V_{water}\,\rho_{water}}{V_{oil}\,\rho_{oil}} + \frac{(K_B)_{water}}{(K_B)_{oil}}}{\frac{V_{water}\,\rho_{water}}{V_{oil}\,\rho_{oil}} + \frac{(K_A)_{water}}{(K_A)_{oil}}}\right) \quad (1)$$

325 Where subscripts *ASW* and *water* represent the original ASW water and water phase after

326 oil-water equilibrium; V_{oil} and V_{water} are the volumes of oil and groundwater involved in the system;

327 ρ_{oil} is the density of oil, which is taken to be 0.9 g/cm^3 and 0.85 g/cm^3 for API=25 and 34

328 respectively; ρ_{water} is the density of groundwater as 1.0g/cm^3; $K_{A(water)}$, $K_{B(water)}$ are Henry's

329 constants of species A and B in the groundwater; $K_{A(oil)}$, $K_{B(oil)}$ are Henry's constants of A and B in

330 the oil. In this study, species A includes ^{20}Ne, ^{84}Kr or ^{130}Xe and species B is ^{36}Ar.

331 *Rayleigh fractionation.*

332 A simple Rayleigh fractionation law is used to model oil-water equilibrium in an open dynamic

333 system (Battani et al., 2000):

334
$$\left(\frac{A}{B}\right)_{water} = \left(\frac{A}{B}\right)_{ASW} f^{(\alpha-1)} \quad (2)$$

335
$$\alpha = \frac{\left(\frac{(K_A)_{water}}{(K_B)_{water}}\right)}{\left(\frac{(K_A)_{oil}}{(K_B)_{oil}}\right)} \quad (3)$$

336 Where f is the fraction of species B remaining in the water phase; α is the fractionation

337 coefficient given by Eq. (3); other parameters are the same as those in Eq. (1). Modelling results of

338 both fractionation models are shown in Fig. 6.

339 Starting with an ASW ratio of ^{20}Ne/^{36}Ar = 0.143, ^{84}Kr/^{36}Ar = 4.02 × 10^{-2} and ^{130}Xe/^{36}Ar = 4.02

340 × 10^{-4}, the Batch fractionation show a maximum ^{20}Ne/^{36}Ar ratio in groundwater when the V_{oil}/V_{water}

341 ratio approaches infinity. The maximum ^{20}Ne/^{36}Ar in groundwater are 0.271 and 0.392 respectively

342 when equilibrating with a light oil phase (API=34) and a heavy oil phase (API=25). From Fig. 6, it

343 is clear that light oil-water fractionation process in a closed system cannot account for all the

344 measured ^{20}Ne/^{36}Ar ratios (0.195 - 0.382). Rayleigh fractionation occurring in a dynamic system,

345 there are no limiting values for elemental ratios when V_{oil}/V_{water} ratio approaches infinity. Although

346 all three fractionation models (heavy oil-water batch fractionation, heavy oil-water Rayleigh

347 fractionation, and light oil-water Rayleigh fractionation) can explain the measured ^{20}Ne/^{36}Ar ratios,

it is apparent that the better fit for the measured ratios is the Rayleigh heavy oil-water fractionation with a maximum additional 600% Xe and 100% Kr. Fig. 6 shows that the observed variation in measured noble gas concentrations is most consistent with the curvilinear trend of Rayleigh heavy oil-water fractionation line. All the $^{20}Ne/^{36}Ar$, $^{84}Kr/^{36}Ar$ and $^{130}Xe/^{36}Ar$ ratios are accounted for by the Rayleigh heavy oil-water fractionation line and with 600% excess Xe and 100% excess Kr.

Previous studies have shown similar Kr and Xe enrichment in natural gas and CO_2 gas fields. For example, the $(^{132}Xe/^{36}Ar)_{meas.}/(^{132}Xe/^{36}Ar)_{air}$ value is up to 576 in gas separated from oil-associated gases from the Elk Hill oil fields, California (Torgersen and Kennedy, 1999) and is approximately 100 in coal bed gases from San Juan Basin (Zhou et al., 2005). Similar heavy noble gas enrichment is also seen in CO_2 gas from the Colorado Plateau and Rocky Mountain provinces, USA (Gilfillan et al., 2008), natural gas from the Sleipner Vest field (Barry et al., 2016) and stray gas preserved in the Trinity aquifer, North-Central Texas (Wen et al., 2017). Heavier noble gase species have been suggested to preferentially adsorb onto organic-rich minerals (Podosek et al., 1981). When buried, these sediments desorb at high temperatures and heavy noble gases are released into the groundwater or free gas phase, causing the enrichment of Kr and Xe relative to Ar in deep fluids (Zhou et al., 2005; Barry et al., 2016). Therefore, various excess of Xe and Kr observed in this study are caused by the variable distribution of organic-rich material.

5.1.4 Oil and groundwater volume ratio in the Weihe Basin

The volume ratio of oil to water is a key parameter to assess oil generation over geological time. The V_{oil}/V_{water} ratio can be calculated based on the model of heavy oil-water Rayleigh fractionation with heavy noble gas excesses. It is suggested that step-wise gas-water equilibrium can approximate Rayleigh fractionation if V_{gas}/V_{water} is small in each stage (Zhou et al., 2005). The principle is the same for the oil-water equilibrium. V_{oil}/V_{water} in one stage equilibration between oil and water phase is given by Battani et al. (2000):

$$\frac{V_{oil}}{V_{water}} = \frac{\rho_{water}}{\rho_{oil}} \frac{(K_{Ar})_{oil}}{(K_{Ar})_{water}} \left(\frac{1-f}{f}\right) \quad (4)$$

Where V_{oil} is the oil volume equilibrating with the groundwater phase; V_{water} is the groundwater

374   volume involved in oil-water equilibration; ρ_{oil} and ρ_{water} are the density of oil and groundwater,

375   which are taken to be 0.9g/cm^3 and 1.0 g/cm^3 respectively. $(K_{Ar})_{water}$ and $(K_{Ar})_{oil}$ are Henry's

376   constants of ^{36}Ar in the groundwater and oil phase respectively. f is the fraction of ^{36}Ar remaining in

377   the residual groundwater.

378   If a small volume of oil (V_{oil}/V_{water} = 3×10^{-5} is chosen, Zhou et al., 2005) equilibrates with

379   groundwater, we can calculate the fraction of ^{36}Ar remaining in the groundwater phase in each

380   single stage (f_{single}). Since excess Kr and Xe have significant impact on the ^{84}Kr/^{36}Ar ratio and

381   ^{130}Xe/^{36}Ar ratio (Section 5.2.3), ^{20}Ne/^{36}Ar ratios are selected to calculate the final fraction of ^{36}Ar (f)

382   remaining in the groundwater after oil-water equilibrium calculated by Eq. (3). The number of

383   single stages of oil/water equilibration (n) can be calculated by $f = f_{single}{}^{\wedge}n$ then the total V_{oil}/V_{water}

384   equals $n\times3\times10^{-5}$. The calculated V_{oil}/V_{water} ratios range between 0.06 and 0.18 (Table 4). Because

385   total degassing during sampling is assumed and the slight elevation of ^{20}Ne/^{36}Ar in sample gas than

386   that in groundwater is not taken into account, the derived V_{oil}/V_{water} values are maxima.

387   Based on the total static reserve of geothermal fluids beyond 4000m in depth in the Weihe

388   Basin (14781.20×10^8 m^3, Zhang et al., 2018b and references therein), the oil volume equilibrating

389   with present groundwater varies from 887×10^8 m^3 to 2661×10^8 m^3. This suggests that abundant oil

390   has been generated in Weihe Basin as these values are even higher than that of URR (ultimately

391   recoverable resources) standard of a mega-giant oil field (78.25×10^8 m^3, Ivanhoe and Leckie, 1993).

392   Given the fact that there are three Palaeogene-Neogene combinations of reservoir and covering

393   strata (Li et al., 2013), it is likely that oil has accumulated in the lithologic traps in the Weihe Basin.

394 **5.2 ^{4}He accumulation**

395 **5.2.1 Relationship between ^{4}He and groundwater**

396   ^{20}Ne in subsurface fluids is derived from ASW without other sources. Since He and Ne have

397   similar Henry's constants in water and oil (Ballentine et al., 2002), the water-oil-gas fractionation

398   results in little fractionation between them. Therefore, ^{4}He/^{20}Ne is an excellent parameter to study

399   the relationship between ^{4}He accumulation and groundwater movement.

400   There is a positive correlation between ^{4}He and ^{20}Ne (R^2=0.84, Fig. 7) for samples in Group A

401   and B with ^{4}He/^{20}Ne ratios varying from 5113 to 9318 except for WR-2 (1439). This is consistent

402   with the assumption that ^{4}He and ^{20}Ne were both exsolved from the water phase during sampling.

403   As the ^{20}Ne/^{36}Ar ratio of WR-2 (0.287) is consistent with those of others (0.195 - 0.382), it excludes

404   the air-contamination possibility for the sample (this is also described in section 4.2.5). The lower

405   ^{4}He/^{20}Ne ratio of WR-2 suggests that some younger groundwater preserved with less or no crustal

406   ^{4}He mixed with the older groundwater. WR-HX has an extremely high ^{4}He/^{20}Ne ratio (37164)

407   compared with samples in Group A and B. This ratio is similar to that observed in helium-rich

408   Hugoton-Panhandle gas field (24871 - 46023, calculated from Ballentine and Lollar, 2002). The

409   data from Hugoton-Panhandle field are shown as squares in Fig. 7. Since groundwater is

410   widely distributed in the subsurface and He is unlikely to be transported by advective flow alone

411   due to its low abundance in the geological environment (Ballentine and Burnard, 2002), it is

412   reasonable to expect that He can migrate in the subsurface together with groundwater movement.

413   The high ^{4}He/^{20}Ne ratio of WR-HX suggests a high ^{4}He flux or low groundwater flow rate. There is

414   no evidence that a low rate of groundwater flow occurs in the area where the WR-HX well is

415   located. Also, WR-HX is located near the uranium and thorium-rich Huashan granitic body.

416   Therefore, it is reasonable to attribute the high ^{4}He/^{20}Ne ratio of WR-HX to the high ^{4}He flux in this

417   area.

418   **5.2.2 ^{4}He concentrations in groundwater**

419   The initial ^{4}He concentrations in groundwater are good parameters to quantify the relationship

420   between ^{4}He and groundwater. For Group A and B samples, when calculating the initial ^{4}He

421   concentrations in groundwater, the volume ratio of gas to groundwater is needed, which can be

422   calculated by:

423
$$\frac{V_{gas}}{V_{water}} = \frac{\left(C_{^{36}Ar}\right)_{water}}{\left(C_{^{36}Ar}\right)_{gas}} \qquad (5)$$

424
$$\left(C_{^{36}Ar}\right)_{water} = \left(C_{^{36}Ar}\right)_{ASW} \times f \qquad (6)$$

425   Where subscripts *water*, *gas* represent the water phase and the gas phase collected from

wellheads during sampling. $\left(C_{36_{Ar}}\right)_{ASW}$ is the concentration of ^{36}Ar in original water (ASW). f is the fraction of ^{36}Ar remaining in the residual groundwater after oil-water fractionation, which can be calculated by Eq. (2). The calculated V_{gas}/V_{water} ratios (under STP conditions) vary from 0.02-0.08 for Group A samples and 1.22-1.38 for Group B samples (Table 4). These vaules provide maximum ratios especially for Group A samples when considering the slight incomplete degassing during sampling caused by the low V_{gas}/V_{water} ratios. The initial helium concentrations in groundwater before oil-water fractionation for Group A and Group B samples can be calculated based on the oil-gas fractionation model, V_{gas}/V_{water} ratios in the subsurface and the ^{4}He concentrations in sampled gases (Table 2). Although the ^{4}He concentrations in Group A samples is higher than those in Group B samples by one order of magnitude, the initial helium concentrations in groundwater are similar for Group A samples ($2.36 - 15.4 \times 10^{-4}$ cm^3 STP/g and 9.05×10^{-4} cm^3 STP/g in average) and Group B samples (9.06 and 12.2×10^{-4} cm^3 STP/g). The low concentrations of He measured in Group B gas samples can be caused by addition of CH$_4$, i.e., the addition of major gas has a strong dilution effect on helium concentration.

If assuming the gas sample collected at well WR-HX was completely dissolved in groundwater in the subsurface, based on the V_{gas}/V_{water} calculation formula (equation 5), the observed 5-12 times higher ^{36}Ar concentration in the WR-HX sample than those in Group B samples would suggest the 5-12 times lower V_{gas}/V_{water} ratio at well WR-HX than Group B wells. However, the gas content of WR-HX well was much larger than in Group B wells, implying that the collected WR-HX gas is not exsolved from groundwater completely and at least part of gas in the WR-HX well is derived from a free gas phase in the subsurface. The high ^{36}Ar concentration in the gas reservoir at WR-HX can then be explained by the exchange of gas contents between groundwater and the gas reservoir. This process would continuously extract ^{36}Ar and ^{4}He from the groundwater into the gas phase and dissolve CH$_4$ from the reservoir into groundwater during the migration of the groundwater.

Since the sampled gas of WR-HX is a mixture of free gas and dissolved gas, two extreme cases are considered to calculate the initial ^{4}He concentrations in groundwater: (1) If the WR-HX sample

452 is derived entirely from groundwater, the initial ^{4}He concentration in groundwater is calculated to

453 be 6.13×10^{-3} cm^3 STP/g following the same calculation procedures as Group A and B samples; (2)

454 If the WR-HX sample is taken from the gas reservoir completely, the noble gas signatures in the

455 WR-HX reservoir are the result of a gas-water equilibrium process. Although it is possible that

456 groundwater in the WR-HX well has equilibrated with an oil phase like Group A and Group B

457 groundwater before contacting the gas reservoir (section 5.1), the involvement of an oil phase is

458 neglected since the ^{20}Ne/^{36}Ar ratio of WR-HX reservoir (0.198) is only slightly higher than the ratio

459 of ASW (0.143), which can be account for by a gas-water fractionation process. Because it is an

460 open system for Group A and Group B groundwater, we assume that the gas reservoir has

461 undergone gas-water equilibrium in an open system as well. Based on the Rayleigh fractionation

462 among ^{4}He, ^{20}Ne and ^{36}Ar during the gas-water equilibrium under reservoir conditions, the ^{4}He

463 concentration in groundwater that is in contact with the gas reservoir for Group C is calculated to be

464 6.39×10^{-3} cm^3 STP/g. No matter gas in WR-HX sample is dissolved in groundwater or from free gas

465 phase underground, there is little difference of ^{4}He concentrations in initial groundwater (6.13×10^{-3}

466 and 6.39×10^{-3} cm^3 STP/g respectively). In addition, due to the existence of free gas phase in

467 WR-HX area, the latter is chosen in the following calculation. The helium content in the

468 groundwater associated with Group C sample is 4-27 times higher than those in groundwater

469 associated with Group A and B samples. Similarly, radiogenic ^{40}Ar* content in groundwater of

470 Group C is around 3-28 times of those of groundwater of Group A and Group B. Therefore, there

471 should be a background ^{4}He and ^{40}Ar* flux for Group A & B samples and an additional ^{4}He and

472 ^{40}Ar* flux for Group C sample.

473 5.2.3 ^{4}He flux

474 ^{4}He is generated from the radiogenic decay of ^{235,238}U and ^{232}Th (Ballentine and Burnard,

475 2002). The ^{4}He in groundwater can be derived from both in-situ production and external flux

476 (Torgersen, 1980; Torgersen and Clarke, 1985; Zhou and Ballentine, 2006). The in-situ ^{4}He

477 production can be expressed as (Torgersen, 1980):

$$\left[^{4}He\right]_{in\ situ\ production} = \frac{\rho \Lambda J_4 (1-\varphi)}{\varphi} t \quad (9)$$

Where ρ is the density of aquifer in g/cm^3; Λ is the ^{4}He transfer efficiency from rock matrix to groundwater; φ is the aquifer porosity; t is groundwater residence time in year. J_4 is radioactive production of ^{4}He in cm^3 STP ^{4}He/g$_{rock}$ year:

$J_4 = 0.2355 \times 10^{-12} [U](1+0.123[Th]/[U]-4)$ (10)

Where $[U]$ and $[Th]$ are the U and Th concentrations in rocks in ppm.

The steady-state external flux of ^{4}He into groundwater can be expressed as (Zhou and Ballentine, 2006):

$$\left[^{4}He\right]_{external\ flux} = \frac{J_4 \cdot \rho \cdot H}{\varphi h} t \quad (11)$$

Where J_4 is radioactive production of ^{4}He given by Eq. (9) in cm^3 STP ^{4}He/g$_{rock}$ year; ρ is average crust density in g/cm^3; H is the average crust thickness in km; h is the aquifer thickness in km; φ is the aquifer porosity; t is groundwater residence time in year.

The parameters used for calculation of ^{4}He accumulation rates in groundwater are listed in Table 5. The values for average crust compositions are taken to be Clark values, cited from Taylor and McLennan (1985). U and Th concentrations of the aquifer are the Clark values as well due to the absence of values in the local rocks (Table 5). The ^{4}He accumulation rate in groundwater from in-situ production and steady-state external flux (upper crust and lower crust) is 7.79×10^{-10} cm^3 STP/g year. The existing ^{4}He concentrations in groundwater for Group A and B samples (2.36 – 15.4×10^{-4} cm^3 STP/g) give groundwater ages of 0.30-1.98Ma (assuming 100% releasing and transfer efficiency from the crust to water), which are consistent with ages of 0.3-1.3 Ma, derived using the ^{81}Kr dating method (Li et al., 2017). The ages are realistic because the calculated ^{4}He groundwater ages are slightly younger than the age of the main geothermal reservoir (Lantian-Bahe Formation), which was deposited during the Pliocene from 2.58Ma to 5.33Ma.

Similarly, the accumulation of helium in groundwater in the WR-HX well (Group C) requires timescales on the order of 8.2 million years, which is clearly not valid since the groundwater age is older than the aquifer age. Therefore, there must be an additional ^{4}He flux for the Group C sample,

which is consistent with the results from the ^{4}He/^{20}Ne ratio in section 5.2.1. The contribution of Huashan granitic body to the ^{4}He accumulation for the Group C sample is considered since it is in close proximity to the sample location. If the average helium accumulation duration of Group B (1.37Ma) is chosen for the Group C sample, the total amount of helium accumulation derived from aquifer and crust is only 1.07×10^{-3} cm^3 STP/g. This suggests that the additional ^{4}He flux from the Huashan granitic body accounts for 83.3% of the total ^{4}He flux.

Since we assume 100% releasing and transfer efficiency for ^{4}He from crust to groundwater, the ages are minimum estimates. Some helium is still preserved in rocks (Tolstikhin et al., 1996; Tolstikhin et al., 2011) or lost during migration. If the maximum groundwater age in Weihe Basin was the same as the aquifer age (2.58Ma), the maximum release and transfer coefficient of ^{4}He from crust and aquifer to groundwater would be calculated to be 76.7%. Alternatively, episodic release of ^{4}He accumulated in ancient rocks over longer time periods can occur, as inferred for radiogenic He release in Yellowstone (Lowenstern et al., 2014). These authors interpreted high helium concentrations to be the result of helium accumulated in Archaean cratonic rocks (more than 2.5 billion years old) liberated over the past two million years by intense crustal metamorphism. The Cenozoic Weihe Basin is a tectonically active basin with many fractures and recorded destructive earthquakes (Mercier et al., 2013). Therefore, it is possible that a portion of ^{4}He was generated in the crust before the formation of the aquifer, and was released and transferred to the groundwater. This process would produce a high ^{4}He flux and result in maximum estimates for ^{4}He accumulation ages.

5.3 The concentration and source of N$_2$ traced by noble gases

Based on the volumetric ratios, N$_2$ contents in groundwater associated with Group A samples and Group B samples are calculated to be 0.020-0.060 cm^{3}STP/g and 0.067-0.340 cm^{3}STP/g respectively. Similarly, the concentrations of CH$_4$ in groundwater are calculated to be 0.001-0.009 cm^{3}STP/g for Group A samples and 0.648-0.959 cm^{3}STP/g for Group B samples (Table 4), suggesting more potential hydrocarbon resources in the Group B area than A. The carbon isotopes of CH$_4$ in samples range between -19.04‰ and -44.46‰ (VPDB) and fall within the expected range

for coal-derived methane (Dai et al., 1992).

The source of N_2 in groundwater is considered. The $N_2/^{36}Ar$ ratio in original ASW is calculated to be 1.14×10^4 based on Henry's constants of N_2 and ^{36}Ar under recharge conditions. After the oil-water Rayleigh fractionation discussed in section 5.1.3, the residual $N_2/^{36}Ar$ ratios in groundwater vary from 1.33×10^4 to 1.84×10^4. The Henry's constants for N_2 in groundwater at recharge and reservoir conditions are calculated from Wilhelm et al. (1977) and that in oil at reservoir conditions is calculated based on the solubility of MK-8 oil in Logvinyuk et al. (1970) (Table 4). The measured $N_2/^{36}Ar$ ratio varies from 5.20×10^4 to 4.62×10^5, which means that only 13.2-30.3% of N_2 in Group A samples and 2.9% - 8.0% in Group B samples are derived from air-saturated water. As the helium isotope ratios are clearly crustal, it is reasonable to exclude a significant contribution from mantle source for N_2. In addition, N_2 can also be released from organic matter during thermal decomposition or from sediments and basement during metamorphism (Danabalan, 2017).

5.4 Helium accumulation model and conditions

5.4.1 Helium accumulation model in the Weihe Basin

The relationship between different sample groups and the constraints on fluid evolution history from noble gas partition modelling are shown in Fig. 8, which illustrates the accumulation of ^4He, CH_4, N_2 and ASW-derived noble gases in the Weihe Basin. Specifically, the process includes four stages:

① ^{20}Ne, ^{36}Ar, other ASW-derived noble gases and N_2 (2.9% - 30.3% of total N_2) from air dissolved into surface water at recharge conditions of 10°C, 0M NaCl and an average altitude of 1000m (North Qinling Belt) were incorporated.

② Crustal radiogenic noble gases (e.g., ^4He and $^{40}Ar^*$) were transferred to the groundwater on a time scale between 0.3 and 1.98 million years. This assumes the releasing and transfer efficiency from source rock to groundwater of ^4He is 100%, therefore the timescales for ^4He accumulation could be longer if efficiency is lower. On the other hand, ^4He accumulation ages could be shorter if

557 there were episodic release of ^{4}He accumulated in ancient rocks, which would produce a high ^{4}He

558 flux.

559 ③ Groundwater underwent heavy oil-groundwater Rayleigh fractionation with V_{oil}/V_{water}

560 being 0.06-0.18. This process caused an increase of $^{20}Ne/^{36}Ar$ ratio (0.195-0.382) in groundwater to

561 values higher than that in ASW (0.143).

562 ④ Addition of different amount of major gases (CH_4 and N_2) resulted in various signatures in

563 the three groups of samples. There are three scenarios.

564 Group A: Minor CH_4 and nitrogen released from organic matter, sediments and/or basement

565 were dissolved into groundwater, result in CH_4 and N_2 concentrations being 0.001-0.009 cm^{3}STP/g

566 and 0.020-0.060 cm^{3}STP/g respectively. The total dissolved gas amount is low (V_{gas}/V_{water} ratios are

567 0.02-0.08), having a minor dilution effect on noble gases in groundwater and causing the high

568 concentration of ^{4}He (32.3 to 294 $\times$ 10^{-4} cm^3 STP/cm^3), high concentration of ^{20}Ne (15.9 to 39.5

569 $\times$10^{-7} cm^3 STP/cm^3) in samples.

570 Group B: Compared with Group A, more CH_4 and N_2 were generated and dissolved into Group

571 B groundwater, making CH_4 and N_2 concentrations in groundwater being 0.648-0.959 cm^{3}STP/g

572 and 0.067-0.340 cm^{3}STP/g respectively. The gas amount dissolved in groundwater is high

573 (V_{gas}/V_{water} ratios are 1.22-1.38) caused a major dilution effect on He and other noble gases

574 concentrations. This process resulted in the low concentrations of ^{4}He (5.74 and 6.21 $\times$ 10^{-4} cm^3

575 STP/cm^3), low concentrations of ^{20}Ne (0.69 to 1.11 $\times$ 10^{-7} cm^3 STP/cm^3) in samples.

576 Group C: Abundant CH_4 and N_2 saturated the groundwater and formed a free gas reservoir.

577 Then continuous gas-water interaction caused partition of less soluble noble gases (e.g., ^{4}He, ^{20}Ne

578 and ^{36}Ar) into the gas phase. This resulted in the high concentration of He (2.11%) in the WR-HX

579 sample compared with those in the Group B samples. The high ^{4}He flux of the WR-HX sample can

580 be accounted for by a background ^{4}He flux shown in Group A & B samples and an additional ^{4}He

581 flux possibly coming from adjacent granitic bodies, which increased the accumulation rate of He.

582 **5.4.2 Conditions for helium accumulation**

The most fundamental condition for high helium accumulation is high He flux. The primary reason why the Group C sample has a high helium concentration is the additional helium flux from the adjacent Huashan granitic body. The granitic bodies and other uranium-rich and thorium-rich rocks are suitable helium source rocks. Therefore, the wells close to these rocks are more likely to accumulate helium. In addition, episodic releasing of ^{4}He preserved in rocks during its geological history could increase He flux significantly during tectonic movement. The rift valley area with good trap conditions could potentially accumulate significant amounts of helium, as observed in the region surrounding the Tanzanian Craton (Danabalan, 2017).

The second condition for economic helium accumulation is the existence of a free gas phase of the major gas component. If there is a gas reservoir (associated with the Group C sample in this study), helium and other noble gases dissolved in groundwater would exsolve into a gas phase continuously rather than migrate elsewhere due to groundwater flow (Group A and B). When groundwater migrates through the reservoir, the free gas phase works like a "filter screen" to concentrate noble gases, especially the less soluble helium, into the gas phase. The different helium concentrations among the groups in our study suggest that the free gas phase plays an important role in accumulating less soluble helium. Dissolved helium is less commercially viable than free helium gas since the production of dissolved gases in groundwater from a geothermal field is generally lower than gas production from a natural gas field.

Finally, He accumulation requires little or no major gas (e.g., CH_4, N_2 and CO_2) supplement after the formation of the free gas phase. The early gas phase in contact with groundwater would acquire most of the helium. If significant major gas migrated along the same pathway into a free gas reservoir, this would dilute the high helium concentration in the gas reservoir formed in the early stages (Brown, 2010). Since the total He content is principally controlled by the He flux and accumulation time, if there was large amount of major gas added, the helium concentration in the gas reservoir or groundwater would be diluted to below industrial grade (0.05 - 0.1 vol%).

6 CONCLUSIONS

23

Helium is a vital and indispensable resource in the fields of nuclear magnetic resonance (NMR), high-tech industry and scientific research. Although, there is an impending helium shortage globally, it has not been widely recognized that helium is an important and valuable by-product in natural gas and geothermal groundwater extraction. The extent of and controls on helium accumulation in geothermal or petroliferous basins are still poorly understood.

In this contribution, groundwater evolution and helium accumulation processes were modelled in the Weihe Basin geothermal field, central China using major gas contents, noble gas components and isotopic ratios, and carbon isotopic ratios. The 12 gas samples can be classified into three groups with distinctive properties, of which: Group A has high concentrations of N_2 and He; Group B has high contents of CH_4 and low contents of He; and Group C has a high content of CH_4 and a low content of He. Noble gas isotopes are predominantly radiogenic and ASW-derived. Modelling suggests that Group A and B samples have undergone a heavy oil-water fractionation in an open system with 600% excess Xe and 100% excess Kr with calculations suggesting there are 887 - 2661 $\times 10^8 \, m^3$ oil generated in the basin during its the geological history.

Current average ^{4}He concentrations dissolved in groundwater for Group A and B samples require the transfer of all helium produced from crust to groundwater over the last 0.30Ma-1.98Ma. The free gas phase is deemed to exist in the subsurface of the WR-HX area (Group C), where the Huashan granitic body provides an additional ^{4}He flux. Based on the elemental ratios of ^{4}He/^{20}Ne, $N_2/^{36}$Ar and contents of ASW-derived noble gases, CH_4 and N_2, the accumulation processes of helium and hydrocarbon in the three sample groups are modelled, which can be explained by a 4-stage process.

There are 3 major controls on the helium accumulation in general. The most important factor is a high He flux, which controls the He accumulation rate. The second factor is the existence of a free gas phase of major gas components (e.g., CH_4, N_2, CO_2), which can strongly apportion helium into the gas phase. Finally, a minimal amount of major gas should be supplied after the formation of the free gas phase since they have a dilution effect on the helium concentration.

REFERENCES

Ballentine C.J., O'nions R., Oxburgh E., Horvath F. and Deak J. (1991) Rare gas constraints on hydrocarbon accumulation, crustal degassing and groundwater flow in the Pannonian Basin. *Earth Planet. Sci. Lett.* **105**, 229-246.

Ballentine C.J., Burgess R. and Marty B. (2002) Tracing fluid origin, transport and interaction in the crust. *Rev. Mineral. Geochem.* **47**, 539-614.

Ballentine C.J. and Burnard P.G. (2002) Production, Release and Transport of Noble Gases in the Continental Crust. *Rev. Mineral. Geochem.* **47**, 481-538.

Ballentine C.J. and Lollar B.S. (2002) Regional groundwater focusing of nitrogen and noble gases into the Hugoton-Panhandle giant gas field, USA. *Geochim. Cosmochim. Acta* **66**, 2483-2497.

Barry P.H., Lawson M., Meurer W.P., Danabalan D., Byrne D.J., Mabry J.C. and Ballentine C.J. (2017) Determining fluid migration and isolation times in multiphase crustal domains using noble gases. *Geology* **45**, 775-778.

Barry P.H., Lawson M., Meurer W.P., Warr O., Mabry J.C., Byrne D.J. and Ballentine C.J. (2016) Noble gases solubility models of hydrocarbon charge mechanism in the Sleipner Vest gas field. *Geochim. Cosmochim. Acta* **194**, 291-309.

662 Bottomley D.J., Ross J.D., Clarke W.B. (1984) Helium and neon isotope geochemistry of some

663   ground waters from the Canadian Precambrian Shield. *Geochim. Cosmochim. Acta* **48**,

664   1973-1985.

665 Brown A.A. (2010) Formation of High Helium Gases: A Guide for Explorationists, AAPG

666   Conference, April 11-14, New Oleans, Louisiana, USA.

667 Cai Z., Clarke R.H., Glowacki B.A., Nuttall, W.J. and Ward, N. (2010) Ongoing ascent to the

668   helium production plateau—Insights from system dynamics. *Resour. Policy* **35**, 77-89.

669 Castro M.C., Goblet P., Ledoux E., Violette S. and Marsily G. (1998) Noble gases as natural tracers

670   of water circulation in the Paris Basin: 2. Calibration of a groundwater flow model using noble

671   gas isotope data. *Water Resour. Res.*, **34**(10), 2467-2483.

672 Dai, J.X., Pei, X.G., Qi, H.F. (1992). Natural Gas Geology of China. Petroleum Industry Press,

673   Beijing.

674 Danabalan D. (2017) Helium: Exploration Methodology for a Strategic Resource. Ph. D. thesis,

675   Durham University.

676 Danabalan D., Gluyas J.G., Macpherson C.G., Abraham-James T.H., Bluett J.J., Barry P.H. and

677   Ballentine C.J. (2016) New High-Grade Helium Discoveries in Tanzania, Goldschmidt

678   Conference, June26 - July 1, Yokohama, Japan.

679 Deng Q.D. and You H.C. (1985) The Structural Activity and Formation Mechanism of the

680   Down-faulted Basins around the Ordos block. Seismological Press, Beijing.

681 Gai H.F., Tian H., Cheng P., Zhou Q., Li T.F., Wang X., Xiao X.M. (2019) Influence of retained

682   bitumen in oil-prone shales on the chemical and carbon isotopic compositions of natural gases:

683   Implications from pyrolysis experiments. *Mar. Pet. Geol.* **101**, 148-161.

684 Gautheron C., Moreira M. (2002) Helium signature of the subcontinental lithospheric mantle. *Earth*

685   *Planet. Sci. Lett.* **199**, 0-47.

686 Gilfillan S.M.V., Ballentine C.J., Holland G., Blagburn D., Lollar B.S., Stevens S., Schoell M. and

687   Cassidy M. (2008) The noble gas geochemistry of natural CO_2 gas reservoirs from the

Colorado Plateau and Rocky Mountain provinces, USA. *Geochim. Cosmochim. Acta* **72**, 1174-1198.

Han W., Li Y., Lu J., Ren Z.L., Xu W. and Song B. (2014) The factors responsible for the unusual content of helium-rich natural gas in the Weihe Basin, Shaanxi Province. *Geol. Bull. China* **33**, 1836-1841 (in Chinese with English abstract).

Holland G., Lollar B.S., Li L., Lacrampe-Couloume G., Slater G.F. and Ballentine C.J. (2013) Deep fracture fluids isolated in the crust since the Precambrian era. *Nature* **497**, 357-360.

Ivanhoe L.F. and Leckie G.G. (1993) Global oil, gas fields, sizes tallied, analyzed. *Oil & Gas J.* **91**, 87-91.

Kennedy B., Hiyagon H. and Reynolds J. (1990) Crustal neon: a striking uniformity. *Earth Planet. Sci. Lett.* **98**, 277-286.

Kipfer R., Aeschbach-Hertig W., Peeters F. and Stute M. (2002) Noble Gases in Lakes and Ground Waters. *Rev. Mineral. Geochem.* **47**, 615-700.

Li J., Pang Z.H., Yang G.M., Tian J., Tong A.L., Zhang X.Y., Hu S.M. (2017) Million-year-old groundwater revealed by krypton-81 dating in Guanzhong Basin, China. *Sci. Bull*. **62**, 1181-1184.

Li X.G. and Ren Y.K. (1986) Effect and characteristics of the neotectonics of the Weihe graben. Research on Modern Crustal Movements, 2. Seismological Press, Beijing.zz

Logvinyuk V. P., Makarenkov V.V., Malyshev V.V. Panchenkov G.M. (1970) Solubility of gases in petroleum products. *Chem. Technol. Fuels Oils*, **6**, 353-355.

Lowenstern J.B., Evans W.C., Bergfeld D. and Hunt A.G. (2014) Prodigious degassing of a billion years of accumulated radiogenic helium at Yellowstone. *Nature* **506**, 355.

Ma Z., Yu J., Su Y., Xie J., Jia X. and Hu Y. (2010) $\delta^{18}O$ shifts of geothermal waters in the central of Weihe Basin, NW China. *Environ. Earth Sci.* **59**, 995-1008.

Mamyrin B.A. and Tolstikhin L.N. (1984) Helium isotopes in nature, Elsevier Sci. Pub., Amsterdam.

Mercier J.L., Vergely P., Zhang Y.Q., Hou M.J., Bellier O. and Wang Y.M. (2013) Structural records of the Late Cretaceous–Cenozoic extension in Eastern China and the kinematics of the Southern Tan-Lu and Qinling Fault Zone (Anhui and Shaanxi provinces, PR China). *Tectonophysics* **582**, 50-75.

Niedermann S., Graf T. and Marti K. (1993) Mass spectrometric identification of cosmic-ray-produced neon in terrestrial rocks with multiple neon components. *Earth Planet. Sci. Lett.* **118**, 65-73.

Nuttall W.J., Clarke R.H. and Glowacki B.A. (2012) The Future of Helium as a Natural Resource. Routledge, London and New York.

Pinti D.L., Castro M.C., Lopez-Hernandez A., Han G., Shouakar- Stash O., Hall C.M. and Ramírez-Montes M. (2017) Fluid circulation and reservoir conditions of the Los Humeros Geothermal Field (LHGF), Mexico, as revealed by a noble gas survey. *J. Volcanol. Geotherm. Res.* **333-334**, 104-115.

Podosek F.A., Bernatowicz T.J. and Kramer F.E. (1981) Adsorption of xenon and krypton on shales. *Geochim. Cosmochim. Acta* **45**, 2401-2415.

Sano Y., Marty B. and Burnard P. (2013) Noble Gases in the Atmosphere. In The Noble Gases as Geochemical Tracers (eds. Burnard P.). Springer Berlin, Heidelberg. pp. 17-31.

Taylor S.R. and McLennan S.M. (1985) The continental crust: its composition and evolution. UnitedStates: Blackwell Scientific, Oxford.

Tolstikhin I., Lehmann B.E., Loosli H.H. and Gautschi A. (1996) Helium and argon isotopes in rocks, minerals, and related ground waters: A case study in northern Switzerland. *Geochim. Cosmochim. Acta* **60**, 1497-1514.

Tolstikhin I., Waber H.N., Kamensky I., Loosli H.H., Skiba V. and Gannibal M. (2011) Production, redistribution and loss of helium and argon isotopes in a thick sedimentary aquitard-aquifer system (Molasse Basin, Switzerland). *Chem. Geol.* **286**, 48-58.

Torgersen T. (1980) Controls on pore-fluid concentration of 4He and 222Rn and the calculation of 4He/222Rn ages. *J. Geochem. Explor.* **13**, 57-75.

741 Torgersen T. and Clarke W.B. (1985) Helium accumulation in groundwater, I: An evaluation of

742   sources and the continental flux of crustal ^{4}He in the Great Artesian Basin, Australia. *Geochim.*

743   *Cosmochim. Acta* **49**, 1211-1218.

744 Torgersen T. and Ivey G.N. (1985) Helium accumulation in groundwater. II: A model for the

745   accumulation of the crustal ^{4}He degassing flux. *Geochim. Cosmochim. Acta* **49**, 2445-2452.

746 Torgersen T. and Kennedy B. (1999) Air-Xe enrichments in Elk Hills oil field gases: role of water in

747   migration and storage. *Earth Planet. Sci. Lett.* **167**, 239-253.

748 USGS (United State Geological Survey) (2018) Mineral Commodity Summaries 2018: Helium by J.

749   E. Hamak. Retrieved from the USGS website:

750   https://minerals.usgs.gov/minerals/pubs/commodity/helium/mcs-2018-heliu.pdf (Accessed 07

751   August 2018)

752 Wang J., Liu C., Gao F., Zhang D., Li Y. and Li Z. (2015a) Pre-Cenozoic geological characteristics

753   and oil-gas significance in Weihe basin, Shaanxi Province. *Geol. Bull. China*. **34**(10),

754   1981-1991 (in Chinese with English abstract).

755 Wang X., Wang T. and Zhang C. (2015b) Granitoid magmatism in the Qinling orogen, central China

756   and its bearing on orogenic evolution. *Sci. China: Earth Sci.* **58**, 1497-1512.

757 Warr O., Lollar B.S., Fellowes J., Sutcliffe C.N., McDermott J.M., Holland, G., Mabry, J.C.,

758   Ballentine C.J. (2018) Tracing ancient hydrogeological fracture network age and

759   compartmentalisation using noble gases. *Geochim. Cosmochim. Acta* **222**, 340-362.

760 Weiss R F. (1968) Piggyback sampler for dissolved gas studies on sealed water samples. *Deep-Sea*

761   *Res. Oceanogr. Abstr.* **15**, 695-699.

762 Wen T., Castro M.C., Ellis B.R., Hall C.M. and Lohmann K.C. (2015) Assessing compositional

763   variability and migration of natural gas in the Antrim Shale in the Michigan Basin using noble

764   gas geochemistry. *Chem. Geol* **417**, 356-370.

765 Wen T., Castro M.C., Nicot J.P., Hall C.M., Pinti D.L., Mickler P., Darvari R. and Larson T. (2017)

766   Characterizing the Noble Gas Isotopic Composition of the Barnett Shale and Strawn Group

and Constraining the Source of Stray Gas in the Trinity Aquifer, North-Central Texas. *Environ. Sci. Technol.* **51**, 6533-6541.

Wilhelm E., Battino R. and Wilcock R.J. (1977) Low-pressure solubility of gases in liquid water. *Chem. Rev.* **77**, 219-262.

Xu X., Ma X. and Deng Q. (1993) Neotectonic activity along the Shanxi rift system, China. *Tectonophysics* **219**, 305-325.

Zhang A., Yang Z., Zhong J. and Mi F. (1995) Characteristics of late quaternary activity along the Southern Border Fault Zone of Weihe Graben Basin. *Quatern. Int.* **25**, 25-31.

Zhang L. (2014a) Geothermal and associated water soluble gas resources exploration and prospect forecast of Weihe Basin. Ph. D. thesis, Chang'an Univ (in Chinese with English abstract).

Zhang M., Tang Q., Cao C., Lv Z., Zhang T., Zhang D., Li Z. and Du L. (2018a) Molecular and carbon isotopic variation in 3.5 years shale gas production from Longmaxi Formation in Sichuan Basin, China. *Mar. Pet. Geol.* **89**, 27-37.

Zhang W., Li Y.H., Wang L., Zhao F.H., Han W., and Song C.G. (2018b) The analysis of helium accumulation conditions and prediction of helium resource in Weihe Basin. *Nat. Gas Geosci.* **29**(2), 236-244 (in Chinese with English abstract).

Zhou Z. and Ballentine C.J. (2006) ^{4}He dating of groundwater associated with hydrocarbon reservoirs. *Chem. Geol.* **226**(3), 309-327.

Zhou Z., Ballentine C.J., Kipfer R., Schoell M. and Thibodeaux S. (2005) Noble gas tracing of groundwater/coalbed methane interaction in the San Juan Basin, USA. *Geochim. Cosmochim. Acta* **69**, 5413-5428.

Zhou Z., Ballentine C.J., Schoell M. and Stevens S.H. (2012) Identifying and quantifying natural CO2 sequestration processes over geological timescales: The Jackson Dome CO2 Deposit, USA. *Geochim. Cosmochim. Acta* **86**, 257-275.

Tables

Table 1 Major gas concentrations and carbon isotopes of gases from geothermal wells in Weihe Basin.

Sample	Location	Sampling method[a]	Depth(m)[b]	Group	Compositions (vol%)						Carbon isotopes (‰)	
					C_1	N_2	CO_2	O_2	C_2	C_{3+}	$\delta^{13}C(CH_4)$	$\delta^{13}C(CO_2)$
Normal samples												
Xi'an Depression												
XP-1	Xingping-Huihao	GWS	-	A	4.35	83.63	4.79	3.11	0.01	0.00	-30.41	-10.50
WG-1	Wugong-Xin1	GWS	-	A	5.12	86.73	3.77	0.12	0.02	0.00	-27.85	-8.06
XY-1	Xianyang-Wen4	GWS	2600-2804	A	3.07	91.66	2.09	0.14	0.01	0.00	-20.60	-8.98
XY-2	Xianyang-Jin1	GWS	2000-4080	A	7.24	58.57	31.69	0.51	0.04	0.01	-25.83	-5.77
XY-3	Xianyang-Sanpu1	GWS	-	A	11.35	73.60	9.36	2.86	0.05	0.01	-32.07	-10.42
Gushi Depression												
WR-051	Huaying-051 well	GWS	1900-2600	A	25.40	66.56	3.82	0.06	0.24	0.08	-	-
WR-2	Weinan-Weire 2	GWS	2000-3800	A	11.90	72.24	7.42	6.85	0.42	0.22	-44.46	-8.23
WR-1	Weinan-Weire 1	GWS	2080-3200	B	69.50	4.85	22.24	0.23	2.57	0.55	-30.23	-5.47
WR-11	Weinan-Weire 11	GWS	2200-3650	B	52.94	27.81	13.56	2.28	2.22	0.91	-19.04	-7.49
WR-HX	Huaxian -Huaxian 2	FT	-	C	71.70	27.20	0.03	0.00	0.57	0.11	-33.47	-
Outlier Samples												
XP-2	Xingping-Xintai	GWS	-	A	2.49	91.53	2.66	0.61	0.02	0.00	-30.59	-9.16
XP-3	Xingping-Jincheng 1	GWS	-	A	2.23	89.48	2.28	3.46	0.01	0.00	-	-

[a] GWS and FT represent that the gas samples are either collected through a gas-water separator (GWS) or a flash tank (FT).
[b] Depth of groundwater reservoir.

Table 2 Noble gas isotope systematics of gases from Weihe Basin[a].

Sample	Group	$^4He\times10^{-4}$	$^{20}Ne\times10^{-7}$	$^{36}Ar\times10^{-6}$	$^{84}Kr\times10^{-8}$	$^{130}Xe\times10^{-10}$	$^3He/^4He$ (R/Ra)[b]	$^{20}Ne/^{22}Ne$	$^{21}Ne/^{22}Ne$	$^{40}Ar/^{36}Ar$	$^{86}Kr/^{84}Kr$	$^{132}Xe/^{130}Xe$
				cm^3 STP/cm^3								
Air[c]		0.05	165	31.43	65.0	36.6	1	9.80	0.029	298.56	0.305	6.6098
Normal Samples												
Xi'an Depression												
XP-1	A	161±2	30.8±0.4	10.41±0.13	21.7±0.83	19.4±0.6	0.033±0.001	9.61±0.15	0.0296±0.0008	368±6	0.316±0.025	6.57±0.21
WG-1	A	237±2	39.5±0.4	13.78±0.27	44.9±1.2	40.2±1.1	0.036±0.001	9.83±0.16	0.0295±0.0009	427±9	0.315±0.017	6.92±0.21
XY-1	A	294±3	53.2±0.6	19.20±0.44	64.8±1.8	17.8±0.5	0.071±0.001	9.83±0.15	0.0297±0.0008	447±11	0.314±0.018	6.66±0.19
XY-2	A	94±1	15.9±0.2	7.18±0.11	23.2±0.54	21.7±0.5	0.048±0.001	10.1±0.2	0.0296±0.0008	447±8	0.286±0.014	6.47±0.17
XY-3	A	153±2	16.4±0.2	7.96±0.12	23.1±0.63	17.5±0.4	0.066±0.001	9.86±0.15	0.0311±0.0008	613±11	0.322±0.022	6.50±0.18
Gushi Depression												
WR-2	A	32.3±0.3	22.4±0.3	7.84±0.09	17.8±0.41	14.5±0.8	0.052±0.001	8.92±0.16	0.0291±0.0008	339±5	0.322±0.014	7.08±0.41
WR-051	A	161±2	31.5±0.4	8.26±0.10	16.6±1.10	16.7±0.6	0.070±0.001	9.81±0.15	0.0301±0.0009	518±8	0.299±0.032	6.47±0.27
WR-1	B	5.74±0.06	0.69±0.02	0.251±0.004	0.87±0.01	0.98±0.05	0.070±0.002	10.9±0.4	0.0307±0.0021	735±13	0.301±0.007	7.00±0.36
WR-11	B	6.21±0.06	1.11±0.03	0.578±0.008	2.07±0.02	2.65±0.09	0.079±0.001	8.94±0.24	0.0292±0.0015	541±9	0.308±0.005	6.74±0.25
WR-HX	C	211±2	5.50±0.07	2.88±0.04	9.95±0.11	8.17±0.72	0.126±0.002	8.68±0.15	0.0385±0.0015	1142±19	0.307±0.005	7.22±0.69
Outliers Samples												
XP-2	A	82.4±0.8	30.8±0.4	16.82±0.39	41.4±0.9	23.2±0.7	0.038±0.001	9.38±0.16	0.0285±0.0007	321±5	0.305±0.013	6.50±0.26
XP-3	A	85.3±0.9	69.1±0.9	22.94±0.40	72.0±1.2	30.4±1.1	0.022±0.001	9.31±0.14	0.0283±0.0007	312±5	0.307±0.009	6.70±0.18

[a] 1σ errors are shown in the table after the plus and minus signs.

[b] $^3He/^4He$ ratios (R) are normalized to the air value Ra = 1.4×10^{-6}.

[c] Noble gas concentrations are cited from Sano et al, (2013). $^3He/^4He$ ratio in air is cited from Mamyrin and Tolstikhin (1984). $^{20}Ne/^{22}Ne$ and $^{21}Ne/^{22}Ne$ ratios in air are cited from Bottomley et al. (1984). $^{40}Ar/^{36}Ar$ ratio in air is cited from Lee et al. (2006). $^{86}Kr/^{84}Kr$ ratio in air is cited from Aregbe et al. (1996). $^{132}Xe/^{130}Xe$ ratio in air is cited from Valkiers et al. (1998).

Table 3 Henry's constants (atm kg/mol) of noble gases and nitrogen at modeling conditions[a].

Condition	Depth (m)	Temperature (℃)	Groundwater Salinity (M NaCl)	Water						Heavy oil (API = 25)					
				Helium	Neon	Argon	Krypton	Xenon	Nitrogen	Helium	Neon	Argon	Krypton	Xenon	Nitrogen
Recharge	0	10	0	2440.12	1975.10	538.11	276.98	156.25	1169.12						
Reservoir	2500	88	0.1	2061.27	2069.94	1206.80	971.72	639.84	1983.84	595.39	585.60	124.34	59.46	25.35	295.74

[a] Henry's constants of noble gases are cited from Ballentine et al. (2002) and references therein; Henry's constants of N_2 in water and oil are calculated from Wilhelm et al. (1977) and Logvinyuk et al. (1970) respectively.

Table 4 Volume ratios of oil to groundwater during fractionation, volume ratios of gas to water in the subsurface, calculated He, N_2 and CH_4 contents in groundwater under modeling conditions and percentages of ASW-derived N_2.

Sample	Group	$^{20}Ne/^{36}Ar$	f ^{36}Ar remaining in groundwater	V_{oil}/V_{water}	V_{gas}/V_{water}	He content in groundwater cm³STP/g	CH_4 content in groundwater cm³STP/g	N_2 content in groundwater cm³STP/g	Measured $N_2/^{36}Ar$	Calculated ASW-derived $N_2/^{36}Ar$	Percentage of ASW-derived N_2
XP-1	A	0.295	0.32	0.13	0.04	8.62×10^{-4}	0.002	0.030	1.62×10^4	8.87×10^4	18.35%
WG-1	A	0.287	0.33	0.13	0.03	9.85×10^{-4}	0.001	0.024	1.60×10^4	6.12×10^4	26.19%
XY-1	A	0.277	0.35	0.12	0.02	9.09×10^{-4}	0.001	0.020	1.57×10^4	5.20×10^4	30.33%
XY-2	A	0.222	0.50	0.08	0.08	9.69×10^{-4}	0.006	0.047	1.41×10^4	8.17×10^4	17.32%
XY-3	A	0.206	0.56	0.07	0.08	1.54×10^{-3}	0.009	0.060	1.36×10^4	1.04×10^5	13.17%
WR-2	A	0.287	0.33	0.13	0.05	2.36×10^{-4}	0.006	0.036	1.60×10^4	9.72×10^4	16.50%
WR-051	A	0.382	0.21	0.18	0.03	8.37×10^{-4}	0.008	0.020	1.84×10^4	9.05×10^4	20.35%
WR-1	B	0.308	0.30	0.14	1.38	1.22×10^{-3}	0.959	0.067	1.65×10^4	2.07×10^5	8.01%
WR-11	B	0.195	0.61	0.06	1.22	9.06×10^{-4}	0.648	0.340	1.33×10^4	4.62×10^5	2.88%

Table 5 Parameters used for calculation of ^{4}He accumulation rate.

^{4}He source	U (ppm)	Th (ppm)	Density (g/cm^3)	Porosity (%)	Thickness (km)	Accumulation rate (cm^3 STP ^{4}He/g H$_2$O year)
In situ-aquifer	2.7	9.6	2.6	0.15	0.2	5.54×10^{-12}
External-General Upper crust	2.8	10.7	2.6	-	18	6.86×10^{-10}
External-Lower crust	0.28	1.07	3.3	-	18	8.71×10^{-11}

Figures and Captions
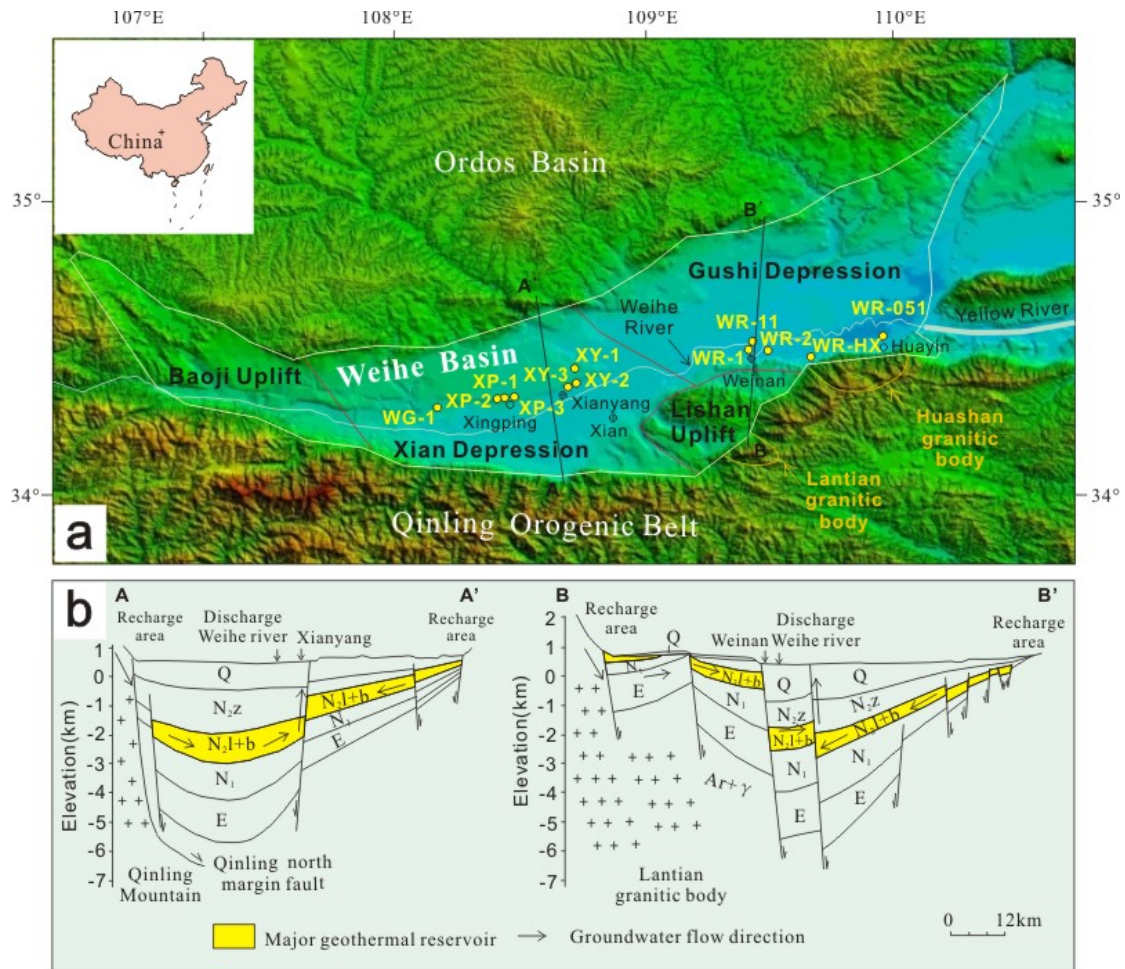
Figure 1 Map of the Weihe Basin. a) shows sample locations (yellow dots), basin area (white line), granitic body region (orange lines), tectonic unit boundaries (red lines) and locations of cross section lines (black lines). The A-A' and B-B' geological cross sections. b) shows the major geothermal reservoir of Pliocene Lantian-Bahe Formation (N_21+b). Groundwater recharges from Ordos Basin and Qinling Orogenic Belt and discharges from the middle Weihe River.
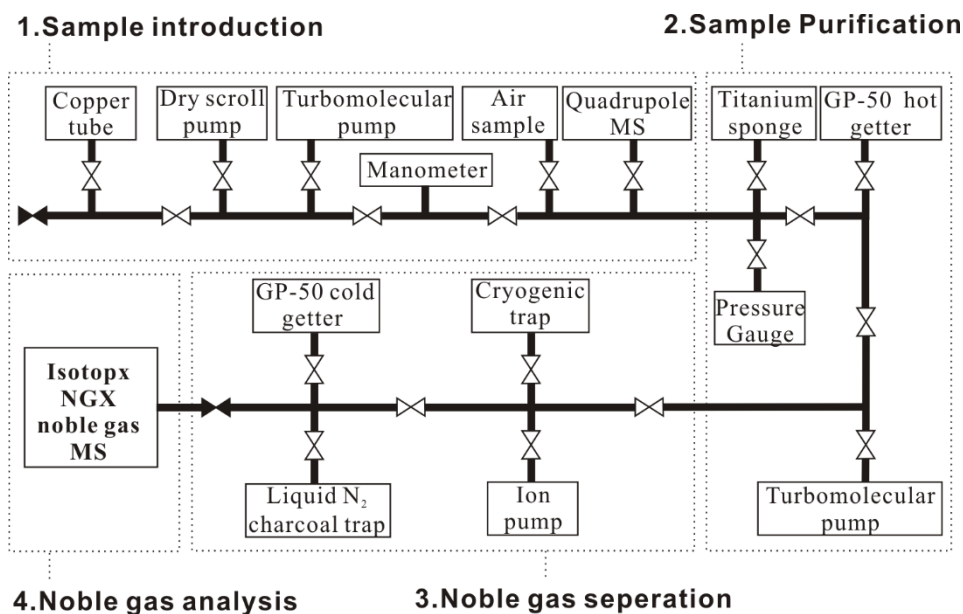
Figure 2 Schematic diagram of the noble gas analytical system at Lancaster University. This system consists of four major sections including sample introduction, sample purification, noble gas separation and noble gas analysis sub-systems. Details of the noble gas analytical procedures are described in Section 3.2.2.
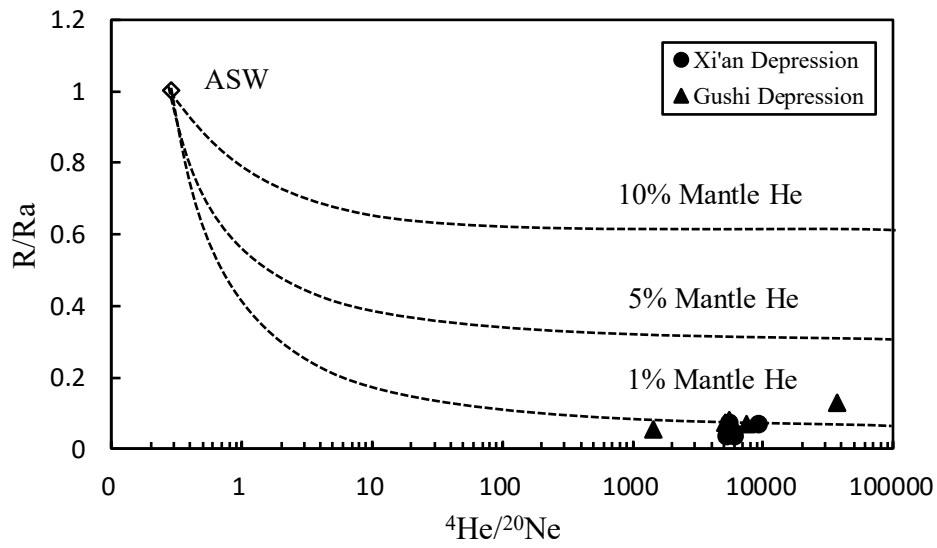
Figure 3 R/R$_a$ ratios vs. ^{4}He/^{20}Ne ratios. Helium is mainly derived from crust with 0.40%-1.94% mantle contribution. The helium isotope endmembers used in this study are the sub-continental lithospheric mantle-like ratio of 6.1R$_a$ from Gautheron and Moreira (2002) and the upper crustal value of 0.008R$_a$ from Ballentine and Burnard (2002).
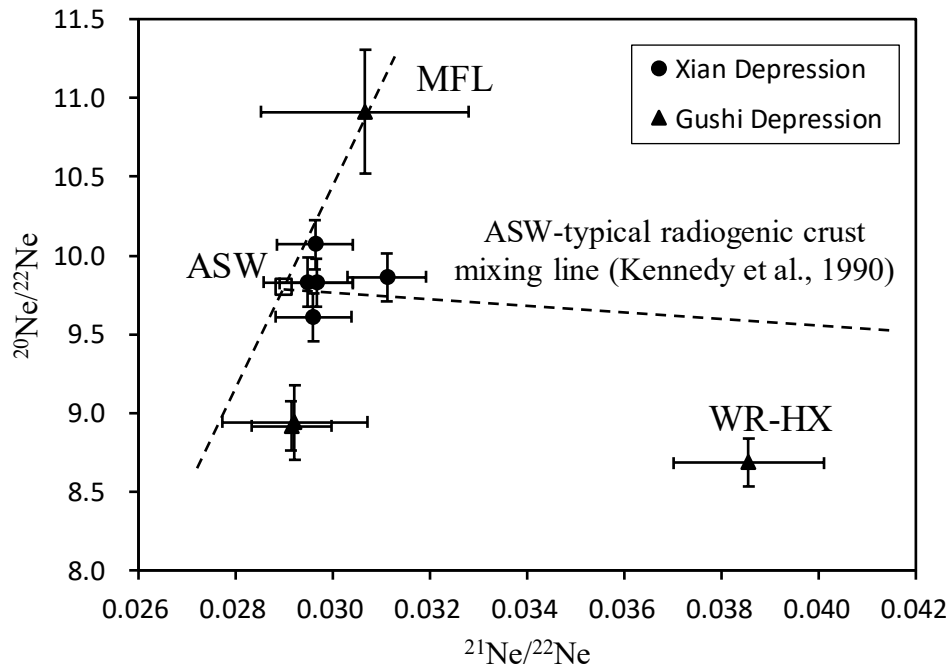
Figure 4 $^{20}Ne/^{22}Ne$ ratios vs. $^{21}Ne/^{22}Ne$ ratios. The data can be accounted for by a small mass fractionation-related process (MFL) and an addition of crustal ^{21}Ne. The calculation of two-component mixing model between ASW and crust ($^{20}Ne/^{22}Ne=0$ and $^{21}Ne/^{22}Ne = 0.47$, Kennedy et al., 1990) suggests that crust-derived ^{21}Ne contributes between 0.00% - 9.47% to the total ^{21}Ne except for WR-HX which is 33.33%.
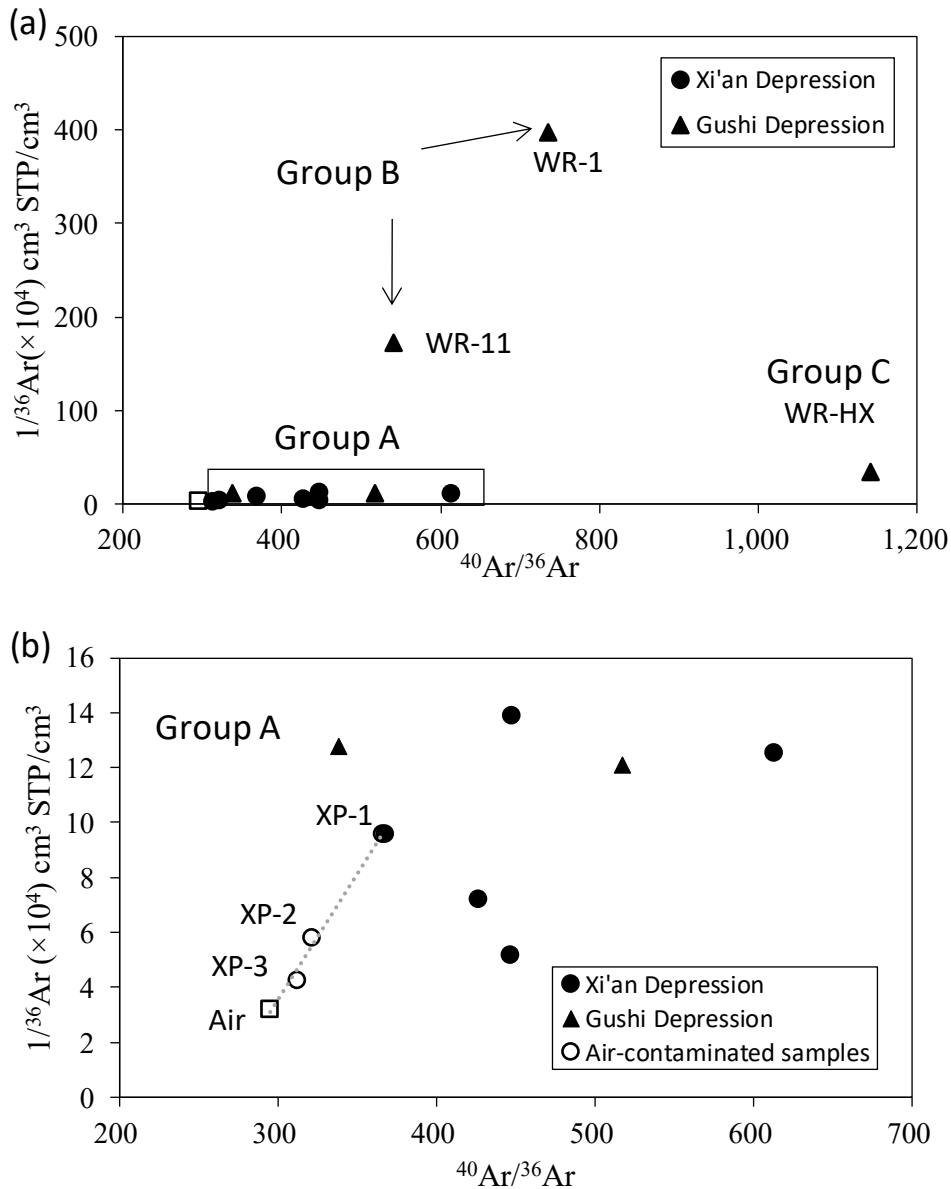
Figure 5 a) ^{36}Ar concentrations ($1/^{36}$Ar) vs. Ar isotopes (^{40}Ar/^{36}Ar) of samples in the three groups. b) shows the detailed characteristics of samples in Group A, in which the samples XP-2 and XP-3 (open circles) are highly consistent with the mixing line of XP-1 (filled circle) and air values (open rectangle), indicating these two samples are likely contaminated by air. There is no positive correlation between ^{40}Ar/^{36}Ar ratios and $1/^{36}$Ar values for the rest of samples.
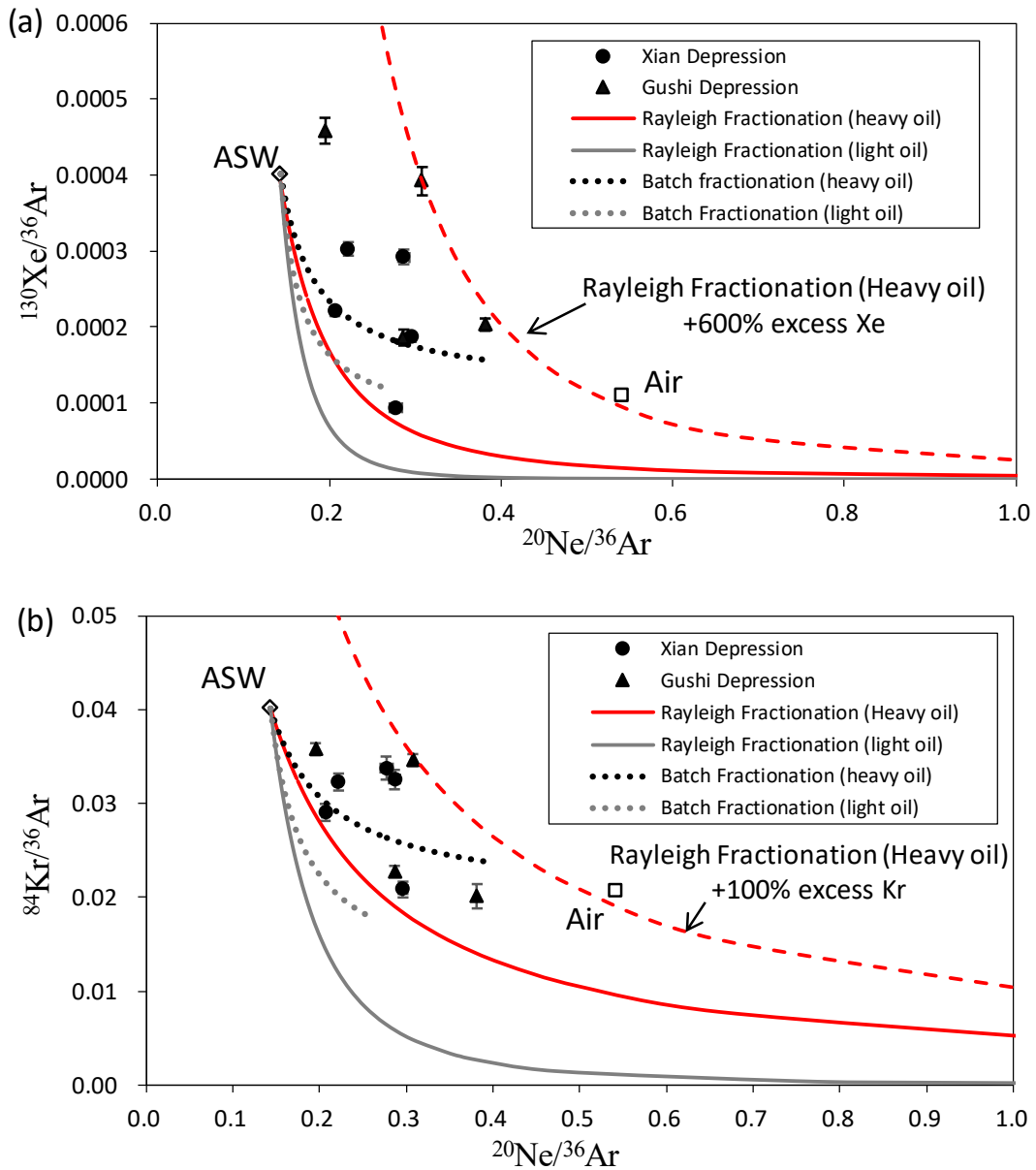
Figure 6 a) $^{20}Ne/^{36}Ar$ vs. $^{130}Xe/^{36}Ar$ and b) $^{20}Ne/^{36}Ar$ vs. $^{84}Kr/^{36}Ar$ remaining in groundwater phase after oil-water Rayleigh fractionation and batch fractionation. The heavy oil-water batch fractionation can explain data better. All data are in the area restricted by the Rayleigh heavy oil-water fractionation line and that with either 600% excess of Xe or 100% excess of Kr. The excess heavy noble gases may be released from organic-rich minerals (Barry et al., 2016; Zhou et al., 2005).
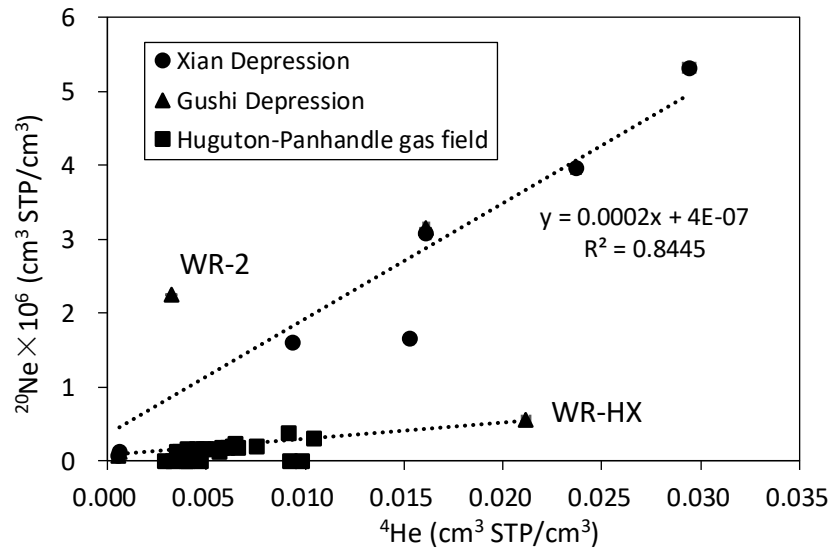
Figure 7 ^{4}He concentrations vs. ^{20}Ne concentrations in samples from Weihe Basin (filled triangles and circles) and Hugoton-Panhandle gas field (filled squares, data from Ballentine and Lollar, 2002). The agreement of ^{4}He and ^{20}Ne concentrations in Group A and B samples (all samples except for WR-HX) suggests helium accumulation is closely related with groundwater migration. The high ^{4}He/^{20}Ne ratio in WR-HX well is similar with those in Hugoton-Panhandle gas field, suggesting a local ^{4}He flux possibly coming from adjacent granitic bodies overlaying the background ^{4}He flux.
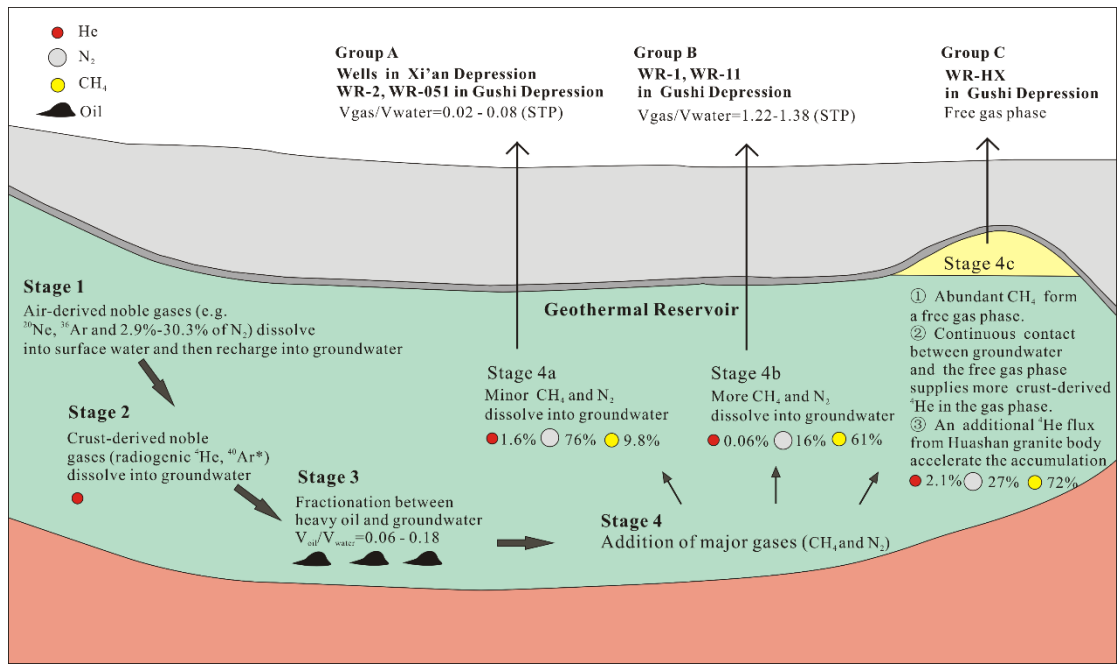
Figure 8 Cartoon illustrating the accumulation process of ^{4}He, ASW-derived noble gases, CH_4 and N_2 in Weihe Basin. See detailed discussion and explanation in Section 5.4.1.